J Mol Model (2013) 19:2189–2195
DOI 10.1007/s00894-013-1762-7

ORIGINAL PAPER

Theoretical study on rate constants for the reactions of $CF_3CH_2NH_2$ (TFEA) with the hydroxyl radical at 298 K and atmospheric pressure

Bhupesh Kumar Mishra · Arup Kumar Chakrabartty · Ramesh Chandra Deka

Received: 6 November 2012 / Accepted: 7 January 2013 / Published online: 25 January 2013

Abstract Theoretical investigations are carried out on reaction mechanism of the reactions of $CF_3CH_2NH_2$ (TFEA) with the OH radical by means of *ab initio* and DFT methods. The electronic structure information on the potential energy surface for each reaction is obtained at MPWB1K/6-31+G(d,p) level and energetic information is further refined by calculating the energy of the species with a Gaussian-2 method, G2(MP2). The existence of transition states on the corresponding potential energy surface is ascertained by performing intrinsic reaction coordinate (IRC) calculation. Our calculation indicates that the H abstraction from $–NH_2$ group is the dominant reaction channel because of lower energy barrier. The rate constants of the reaction calculated using canonical transition state theory (CTST) utilizing the *ab initio* data. The agreement between the theoretical and experimental rate constants is good at the measured temperature. From the comparison with $CH_3CH_2NH_2$, it is shown that the fluorine substution decreases the reactivity of the C-H bond.

Keywords Gas phase reactions · G2(MP2) · H abstraction rate constants · IRC calculation · TFEA

Introduction

Amines are the well-known basic volatile organic compounds identified in the atmosphere in both gas and particulate phases [1–4]. Gaseous amines can contribute to the formation of new particle and secondary organic aerosol by either acid–base reactions with gas-phase acids like HNO_3, H_2SO_4 etc. [5] or oxidation reactions with atmospheric oxidants such as OH, NO_3 and O_3 [6–9]. Amines have attracted a great deal of attention in recent decades, as some field observations [10] and quantum chemical calculations [11, 12] suggested that secondary organic aerosol generated from amines greatly impacts on climate, visibility and human health [13, 14]. Amines can be emitted directly into the atmosphere by a variety of widespread biogenic and anthropogenic sources including automobile exhaust [15], carbon capture and storage [16, 17], animal husbandry [18], aquatic sources [19] and waste incineration and sewage treatment [20]. In the atmosphere, OH, Cl, and NO_3 radicals may react with saturated aliphatic amines via hydrogen abstraction either from the carbon or the nitrogen position. The hydrogen abstraction will result in the formation of an alkyl or an alkylamino radical species that will promptly react further to produce a wide range of closed shell products like amides, nitrosamides, aldehydes, nitrosamines, nitramines in both gas and aqueous phase which may contribute significantly to increase the organic nitrogen fraction of the atmospheric aerosol. Among the degradation products of amines, nitrosamines and nitramines have shown potential carcinogenic activity in both gas and aqueous phases. [16, 21]. It is therefore, important to establish the roles of amines degradation product formation mechanisms with atmospheric conditions. An understanding of the atmospheric oxidation mechanism of amines has long been cited as the most critical needed for further development of reaction mechanisms for the urban and regional atmosphere. Useful properties of compounds containing amines and their negative impact on environment and human health have motivated many studies on their oxidation process. The dominant atmospheric fate of these species is reaction with the OH radical.

Electronic supplementary material The online version of this article (doi:10.1007/s00894-013-1762-7) contains supplementary material, which is available to authorized users.

B. K. Mishra · A. K. Chakrabartty · R. C. Deka (✉)
Department of Chemical Sciences, Tezpur University, Napaam, Tezpur, Assam 784 028, India
e-mail: ramesh@tezu.ernet.in

Table 1 Thermochemical data for the H abstraction reaction channels of $CF_3CH_2NH_2$ calculated at MPWB1K/6-31+G(d,p) level of theory kcal mol^{-1}

Reaction channels	$\Delta_rH°$ kcal mol^{-1}	$\Delta_rG°$ kcal mol^{-1}	$\Delta G^{\#}$ kcal mol^{-1}	$\Delta S^{\#}$ cal mol^{-1} K^{-1}
Reaction 1	−12.85	−14.24	9.74	−28.94
Reaction 2	−10.60	−11.92	10.07	−27.13

The reaction of OH radical with $CF_3CH_2NH_2$ is thought to proceed via hydrogen atom abstracted from either a -NH_2 group or-CH_2 group. So the two primary processes have been considered for the title reaction as given by Reactions (1–2) during the present investigation.

$$CF_3CH_2NH_2 + OH \rightarrow CF_3CH_2NH + H_2O \quad (1)$$

$$CF_3CH_2NH_2 + OH \rightarrow CF_3CHNH_2 + H_2O \quad (2)$$

In this work we focus our attention on the following basic issues:

i. The H abstraction reaction mechanism including OH radical
ii. The features of potential energy surface at the high level of theory including barrier height and thermochemical data

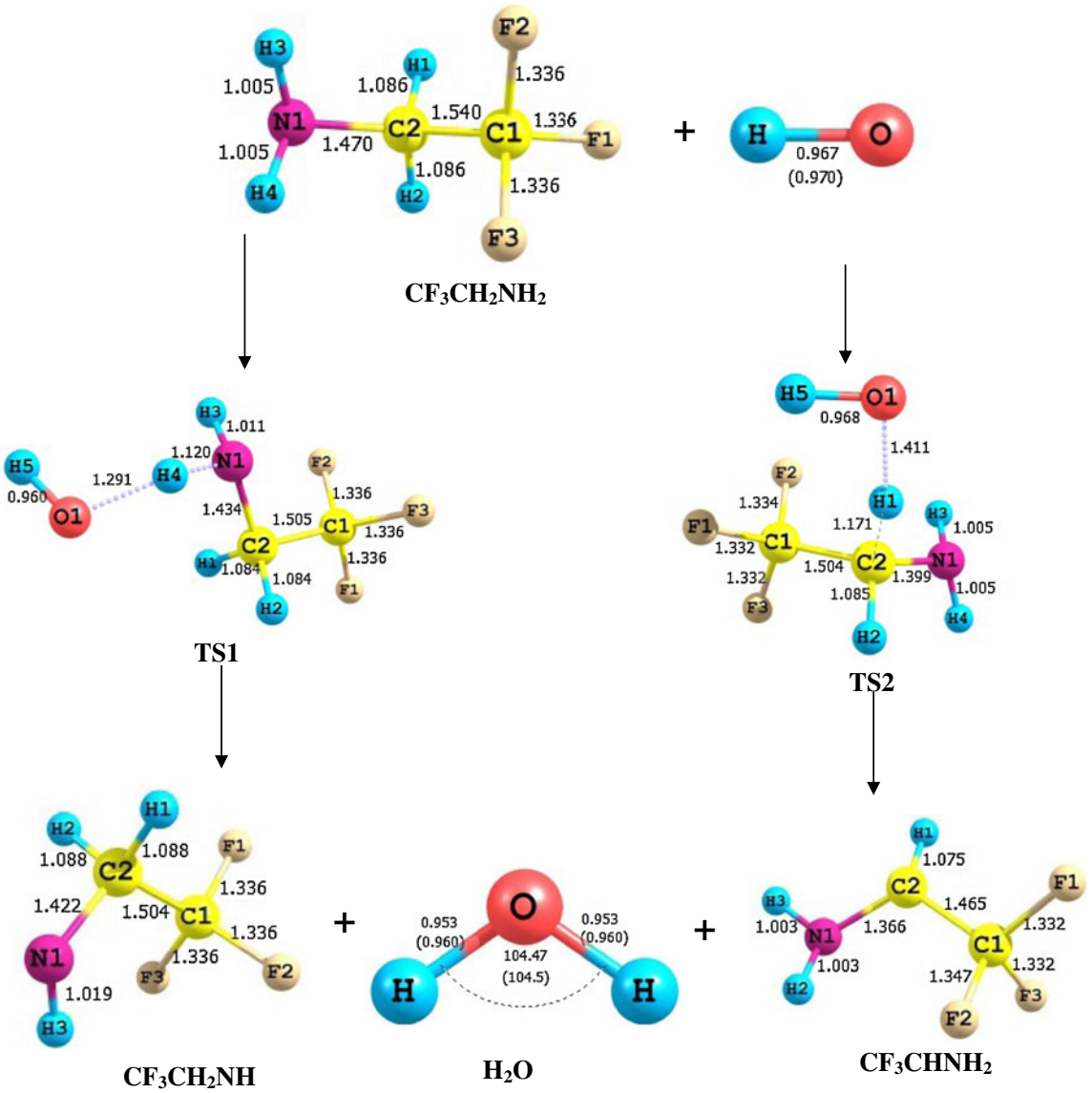

Fig. 1 Optimized geometries of reactants, products and transition states involved in the H abstraction reactions of $CF_3CH_2NH_2$ by OH radical using MPWB1K/6-31+G(d,p) method. The experimental values are given in parentheses

Table 2 Unscaled vibrational frequencies of reactants, products and transition states at MPWB1K/6-31+G(d,p) level of theory and the experimental values are shown in parenthesis

Species	Vibrational frequencies (cm^{-1})
$CF_3CH_2NH_2$	119, 221, 279, 385, 423, 540, 554, 666, 820, 889, 898, 1141, 1192, 1248, 1308, 1337, 1425, 1457, 1503, 1712, 3159, 3218, 3649, 3749
TS1	***1463i,*** 28, 100, 109, 185, 196, 358, 381, 460, 543, 561, 640, 737, 807, 873, 962, 1144, 1160, 1242, 1299, 1330, 1375, 1462, 1518, 1604, 1700, 3134, 3230, 3640, 3937
TS2	***636i,*** 57, 118, 150, 179, 224, 260, 401, 428, 516, 555, 562, 668, 750, 862, 912, 1135, 1175, 1248, 1270, 1288, 1341, 1385, 1464, 1540, 1690, 3222, 3693, 3814, 3887,
CF_3CH_2NH	92, 212, 223, 423, 535, 558, 672, 861, 910, 1101, 1151, 1244, 1285, 1330, 1336, 1448, 1477, 3084, 3176, 3537
CF_3CHNH_2	92, 235, 291, 407, 438, 532, 571, 591, 638, 677, 865, 1106, 1154, 1269, 1302, 1335, 1566, 1696, 3329, 3687, 3813
OH	3868 (3735)[a]
H_2O	1637, 3975, 4101 (1595, 3657, 3756)[a]

[a] From ref. 32

iii. The rate constants of each reaction channel.
iv. The effect of electron withdrawing group at the reactivity of C-H bond.

Literature survey reveals that no theoretical study is performed for this reaction yet. Thus, it is desirable to perform theoretical study utilizing DFT method. In the present study, we have theoretically investigated the kinetics of hydrogen atom abstraction reactions of $CF_3CH_2NH_2$ with OH radical. Canonical transition state theory (CTST) is also utilized to predict the rate constant of the title reaction on the basis of *ab initio* data obtained during the present investigation.

Computational methods

Ab initio quantum mechanical calculations were performed with the Gaussian 09 suite of program [22]. Geometry optimization of the reactant, products and transition states were made at the MPWB1K level of theory [23] using 6-31+G(d,p) basis set. The hybrid meta-density functional, MPWB1K has been found to give excellent results for thermochemistry and kinetics and is known to produce reliable results [24, 25]. In order to determine the nature of different stationary points on the potential energy surface, vibrational frequencies calculations were performed using the same level of theory at which the optimization was

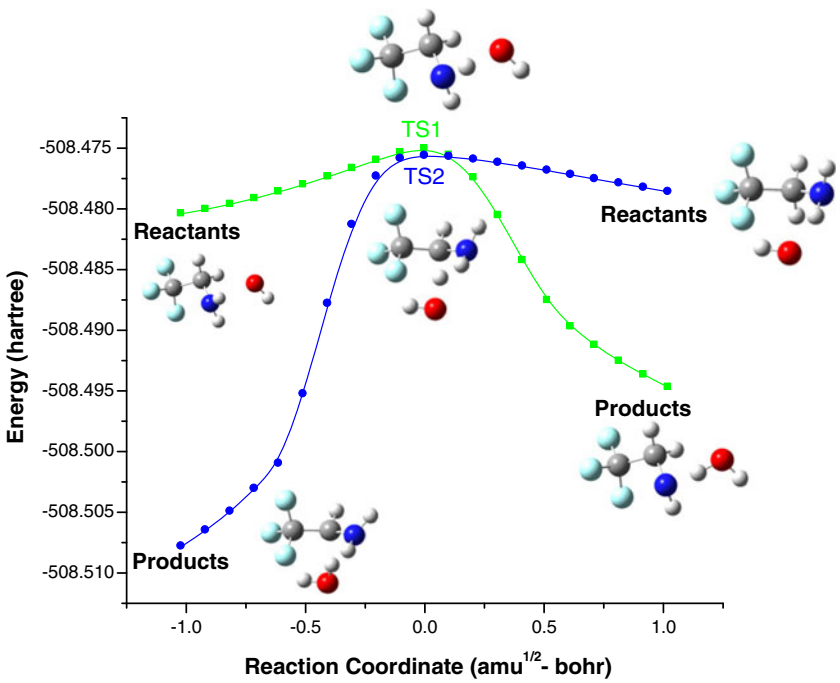

Fig. 2 IRC plots for the transition states TS1 and TS2 involved in $CF_3CH_2NH_2$ + OH reactions at MPWB1K/631+G (d,p) level of theory. The reactants, transition states and products are also shown along the reaction path

Table 3 Comparison of energies (Hartree) of reactants, transition states and products obtained in IRC calculations performed at MPWB1K/6-31+G(d,p) level of theory with the individually optimized values at MPWB1K/6-31+G(d,p) level of theory

Species	IRC	MPWB1K/6-31+G(d,p)
Reactants ($CF_3CH_2NH_2$+ OH)	−508.4804	−508.4811
TS1	−508.4750	−508.4750
Products (CF_3CH_2NH + H_2O)	−508. 4946	−508.4998
Reactants ($CF_3CH_2NH_2$+ OH)	−508.4785	−508.4811
TS2	−508.4756	−508.4756
Products (CF_3CHNH_2+ H_2O)	−508.5078	−508.5076

made. All the stationary points had been identified to correspond to stable minima by ascertaining that all the vibrational frequencies had real positive values. The transition states were characterized by the presence of only one imaginary frequency (NIMAG=1). To ascertain that the identified transition states connect reactant and products smoothly, intrinsic reaction coordinate (IRC) calculations [26] were performed at the MPWB1K/6-31+G(d,p) level. As the reaction energy barriers are very sensitive to the theoretical levels, the higher-order correlation corrected relative energies along with the density functional energies are necessary to obtain theoretically consistent reaction energies. Therefore, a potentially high-level method such as G2(MP2) has been used for single-point energy calculations. The G2(MP2) [27] energy is calculated in the following manner:

$$E[G2(MP2)] = E_{base} + \Delta E(MP2) + HLC + ZPE$$

where, $E_{base} = E[QCISD(T)/6-311G(d,p)]$,

$\Delta E(MP2) = E[MP2/6-311+G(3df,2p)] - E[MP2/6-311G(d,p)]$, and

HLC (High Level Correction) $= -0.00481n_\beta - 0.0001\,9n_\alpha$ (n_α and n_β are the number of α and β valence electrons with $n_\alpha \geq n_\beta$) and ZPE = zero-point energy.

In this method the geometry and frequency calculations were performed at MPWB1K/6-31+G(d,p) level. The ZPE thus obtained was corrected with a scale factor of 0.9537 to partly eliminate systematic errors [23]. A quadratic CI calculation including single and double substitutions with a triples contribution to the energy has also been performed using MPWB1K/6-31+G(d,p) optimized geometries. This dual level calculation (G2(MP2)//MPWB1K) is known to produce reliable kinetic data.

Results and discussion

The detailed thermodynamic calculations performed at MPWB1K/6-31+G(d,p) level for reaction enthalpies, free energies, free energies of activation and entropy of activation associated with reaction channels (1–2) are listed in Table 1. The calculated free energy values as recorded in Table 1 reveal that both reaction channels are exergonic ($\Delta G<0$) and thermodynamically facile at 298 K. The reaction enthalpies value obtained from BHandHLYP calculations is found to be close to the MPWB1K value and amounts to −12.52 and −10.29 kcalmol^{-1}, respectively, for reaction channels (1–2). The optimized geometries of reactants, products and transition states along with structural parameters obtained at MPWB1K/6-31+G(d,p) level are shown in Fig. 1. It can be seen that the calculated bond distances and angle for OH, and H_2O at MPWB1K level show good mutual agreement with the corresponding experimental values [28, 29]. Transition states searched on the potential energy surfaces of reactions (1–2) are characterized as TS1 and TS2, respectively. The search was made along the minimum energy path on a relaxed potential energy surface. We should mention here that reactants, transition states and products are also optimized with BHandHLYP/6-311++G(2d,2p) [30, 31] level to cross check the MPWB1K structure. All the optimized geometries and structural parameters for reactants, TSs and products at BHandHLYP/6-311++G(2d,2p) are given in supporting information Fig. S1 and Table S1. The breaking N-H/C-H and the forming O-H bond length obtained from the two methods were found to be close to each other. Therefore, the structural parameters obtained from computationally cheaper MPWB1K method were used for all energetic and kinetic calculations. In the TS, the important structural parameters that have to be observed are one of the bond lengths of the leaving hydrogen and the newly formed bond between H and O atoms in the OH radical. The TS1 structure for H abstraction by OH radical as shown in Fig. 1

Table 4 Zero-point corrected total energy for the reactants, products and transition states along with the associated energy barrier, ΔE (kcal mol^{-1}). All other values are in hartree

Species	QCISD(T)/6-311 G(d,p)	ΔE	G2(MP2)	ΔE
$CF_3CH_2NH_2$ + OH	−507.6048545	0.00	−507.977131	0.00
TS1	−507.5985214	3.97	−507.9746774	1.53
TS2	−507.5961329	5.47	−507.9732313	2.44
CF_3CH_2NH + H_2O	−507.6244531	−12.29	−508.0042433	−17.01
CF_3CHNH_2+ H_2O	−507.6349939	−18.91	−508.0170061	−25.02

followed by visualization of the optimized geometry using ChemCraft [32] reveals that the breaking bond N-H (N1-H4) increases from 1.005 to 1.120 Å (11 % increase) whereas the newly formed H-O bond (H4-O1) is increased from 0.953 to 1.291 Å resulting in an increase of about 35 %. The fact that the elongation of the forming bond is larger than that of the breaking bond indicates that the barrier of the reaction is near the corresponding reactants. This means the reaction will proceed via early transition state structure which is in consonance with Hammond's postulate [33] applied to an exothermic hydrogen abstraction reaction. While for the H abstraction from $–CH_2$ group (TS2), the elongation of the breaking C-H bond (C2-H1) is found to be 1.086 to 1.171 Å resulting in an increase of about 8 %. The forming H-O bond (H1-O1) is elongated by 0.953 to 1.411 Å (48 %) with respect to the equilibrium bond length in an isolated molecule H_2O. The elongation of the forming bond is greater than that of the breaking bond indicating that the TS is reactant like, i.e., the reaction will proceed via early TS.

Results obtained during frequency calculations for reactants, products and transition states involved in reactions (1–2) at MPWB1K and BHandHLYP levels of theory are recorded in Table 2 and Table S1 of Supporting information. These results show that the reactants and products have stable minima on their potential energy surface characterized by the occurrence of only real positive vibrational frequencies while transition states, TS1 and TS2 are characterized by the occurrence of only one imaginary frequency at 1463 and 636 cm^{-1}, respectively at MPWB1K whereas at BHandHLYP respective values are 1999 and 1465 cm^{-1}. For the species of products, the calculated frequencies are in good agreement with the experimental values [34]. Their good agreements confirm the accuracy and reliability of the calculated rate constants. These vibrational frequencies are analyzed using ChemCraft visualization program [32]. Visualization of the imaginary frequency gives a qualitative confirmation of the existence of transition states connecting reactants and products. For the two H abstraction reactions, TS1 possesses a larger absolute value of the imaginary frequency, 1463i, which indicates that the width of the potential barrier might be narrower and the tunneling effect may be more important in the calculation of the rate constant. Intrinsic reaction path calculations (IRC) [26] have also been performed for each transition state at the same level of theory using the Gonzalez-Schlegel steepest descent path in the mass-weighted Cartesian coordinates with a step size of 0.01 ($amu^{1/2}$- bohr). The IRC plots for TS1 and TS2 shown in Fig. 2 reveal that the transition state structures smoothly connect the reactant and the product sides. The energies of reactants, transition states and products obtained in the IRC calculations performed at MPWB1K/6-31+G(d,p) level of theory are given in Table 3 and they are in excellent agreement with the individually optimized values at MPWB1K/6-31+G(d,p) level of theory.

Single point energy calculations of various species involved in the two H abstraction reactions (1–2) were performed at Møller-Plesset perturbation theory (MP2) using standard and extended basis sets. Calculated total energies are corrected for zero-point energy with a scale factor of 0.9537 [23] obtained at MPWB1K/6-31+G(d,p). Zero-point corrected total energies for various species and transition states involved in the title reactions calculated at QCISD(T) and G2(MP2) are recorded in Table 4. The associated energy barrier corresponding to reactions (1–2) are also recorded in Table 4. To ascertain the accuracy of the G2(MP2)//MPWB1K calculated barrier heights for H- abstraction from the $–NH_2$ and $–CH_2$ groups of TFEA, we have also calculated barrier heights at CCSD(T)/6-311++G(2d,2p)//BHandHLYP/6-311++G(2d,2p) level. The calculated total energies for reactants, transition states and products along with barrier heights are recorded in Table S3 in Supporting information. Our CCSD(T) calculated barrier heights for $–NH_2$ and $–CH_2$ sites amount to 3.00 and 4.80 $kcal mol^{-1}$, respectively. Thus, it seems that the CCSD(T) calculated barrier heights are almost 1.4 $kcal mol^{-1}$ higher than the values calculated at G2(MP2) level. Moreover, the CCSD(T) calculated barrier heights for reaction channels (1–2) are slightly lower that the values calculated at QCISD(T)/6-311G(d,p) level. However, our calculated barrier heights at CCSD(T) level for H-abstraction from $–NH_2$ and $–CH_2$ sites for TFEA are higher than the values for corresponding sites for $CH_3CH_2NH_2$ (ethylamine) reported by Galano and Idaboy [35] at same level of theory.

A schematic potential energy surface of the $CF_3CH_2NH_2$ + OH reactions obtained at the G2(MP2)//MPWB1K/6-31+G(d,p) level is plotted in Fig. 3. In the construction of energy diagram, zero-point corrected total energies as recorded in

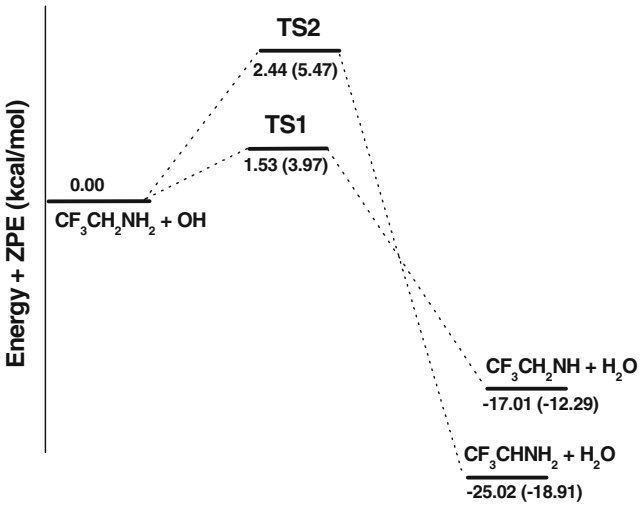

Fig. 3 Schematic potential energy diagram of the title reaction at G2(MP2)//MPWB1K/6-31+G(d,p). The values in parentheses are calculated at QCISD(T)/6-311G(d,p) level. All energy values are in $kcal mol^{-1}$

Table 3 are utilized. These energies are plotted with respect to the ground state energy of $CF_3CH_2NH_2$ + OH arbitrarily taken as zero. The values in parentheses shown in Fig. 3 are ZPE corrected values obtained at MPWB1K/6-31+G(d,p) level. The barrier height for H abstraction from $–NH_2$ group is considerably lower than that from $–CH_2$ group and the dominance of the H abstraction from $–NH_2$ group in the degradation of the TFEA in the atmosphere is thus envisioned. It is seen that the barrier heights of the H- abstraction from $–CH_2$ group in $CF_3CH_2NH_2$ by OH radical at three levels are higher than those of the H- abstraction from the corresponding site in $CH_3CH_2NH_2$ [35]. This indicates that the fluorine atom substitution for hydrogen atom on carbon atom reduces the reactivity of C-H toward H abstraction. It is in line with the earlier conclusion from the reactions of OH with $CF_3CH_2OCHF_2$ /$CH_3CH_2OCH_3$ [36] and CH_3OCH_3/ CF_3OCH_3 [37]. Spin contamination is not important for the $CF_3CH_2NH_2$ because $< S^2 >$ is found to be 0.76 at MPWB1K/6-31+G(d,p) before annihilation that is only slightly larger than the expected value of$<S^2>$= 0.75 for doublets.

Rate constants

The rate constant for reactions (1–2) is calculated using canonical transition state theory (CTST) [38] that involves a semi-classical one-dimensional multiplicative tunneling correction factor given by the following expression:

$$k = \sigma\Gamma(T)\frac{k_B T}{h}\frac{Q^{\ddagger}_{TS}}{Q_R}\ exp\frac{-\Delta E}{RT}, \quad (3)$$

where σ is the symmetry number, Γ(T) is the tunneling correction factor at temperature T. $Q^{\ddagger}_{TS}$ and Q_R are the total partition functions for the transition states and reactants, respectively. ΔE, k_B and h are the barrier height including ZPE, Boltzmann's and Planck's constants, respectively. The partition functions for the respective transition states and reactants at 298 K are obtained from the vibrational frequency calculation made at MPWB1K/6-31+G(d,p) level. In the calculation of electronic partition function, the excited state of the OH radical is included, with a 140 cm^{-1} splitting due to spin-orbit coupling. Barrier heights were estimated from the energy difference including ZPE between TSs and reactants. Calculation for the tunneling correction factor Γ(T) was made using the expression of Wigner [39] as given by the following expression:

$$\Gamma(\mathrm{T}) = 1 + \frac{1}{24}\left(\frac{\mathrm{h}\nu^{\#}}{\mathrm{k_B T}}\right)^2, \quad (4)$$

where $\nu^{\#}$ is the imaginary frequency at the saddle point. The tunneling correction factor Γ(T) is found to be 3.08 and 1.39 for TS1 and TS2, respectively. The partition functions for the respective transition state and reactants at 298 K are obtained from the vibrational frequencies calculation made at MPWB1K/6-31+G(d,p) level.

The rate constants for H atom abstraction reactions from $–NH_2$ and $–CH_2$ groups as given by reactions (1–2) are calculated to be 1.107×10^{-12} and 2.32×10^{-14} cm^3 $molecule^{-1}$ s^{-1} at 298 K and 1 atm, respectively. The overall rate constant corresponding to $CF_3CH_2NH_2$+OH can be calculated as the sum of the rate coefficients of each channel. The calculated overall rate constant (1.13×10^{-12} cm^3 $molecule^{-1}$ s^{-1}) at 298 K is in very good agreement with the available experimental value of $(0.9\pm0.3)\times10^{-12}$ cm^3 $molecule^{-1}$ s^{-1} reported by Koch et al. [40]. However, our calculated rate constant for reaction (2) is lower than the rate constant for the corresponding site for $CH_3CH_2NH_2$ + OH reaction reported by Galano and Idaboy [35]. This is in line with the fact that the substitution of H atoms by F atoms lowers the reactivity of C-H bond.

Conclusions

The potential energy surface and reaction kinetics of the H abstraction reaction systems of $CF_3CH_2NH_2$ + OH [reactions (1–2)] are investigated at G2(MP2)//MPWB1K/6-31+G(d,p) level of theory. The barrier heights for this pathway are calculated to be 1.53 and 2.44 $kcalmol^{-1}$, respectively at G2(MP2) level. The rate constant of the H abstraction reaction calculated by canonical transition state theory with Wigner's tunneling correction is consistent with the available experimental values. Our calculated results reveal that the H abstraction reaction from $–NH_2$ group is a more important degradation channel for $CF_3CH_2NH_2$ in atmosphere. Substitution of H atoms in $CH_3CH_2NH_2$ by fluorine atoms reduces the reactivity of the C-H bond and as a result, the rate constants for H abstraction reaction from $–CH_2$ group in $CF_3CH_2NH_2$ + OH become smaller than that of $CH_3CH_2NH_2$ + OH reaction.

Acknowledgments One of the authors, BKM is thankful to University Grants Commission, New Delhi for providing Dr. D. S. K. Post doctoral fellowship.

References

1. Grönberg L, Lövkvist P, Jönsson J (1992) Chromatographia 33:77–82
2. Gibb SW, Mantoura RFC, Liss PS (1999) Global Biogeochem Cycles 13:161–178
3. Müller C, Iinuma Y, Karstensen J, Van Pinxteren D, Lehmann S, Gnauk T, Herrmann H (2009) Atmos Chem Phys 9:9587–9597
4. Pratt K, Hatch L, Prather K (2009) Environ Sci Technol 43:5276–5281
5. Angelino S, Suess D, Prather K (2001) Environ Sci Technol 35:3130–3138
6. Silva PJ, Erupe ME, Price D, Elias J, Malloy QGJ, Li Q, Warren B, Cocker DR (2008) Environ Sci Technol 42:4689–4896

7. Malloy QJ, Warren B, Li Q, Cocker DR, Erupe ME, Silva PJ (2009) Atmos Chem Phys 9:2051–2060
8. Zahardis J, Geddes S, Petrucci GA (2008) Atmos Chem Phys 8:1181–1194
9. Atkinson R, Perry RA, Pitts JN (1977) J Chem Phys 66:1578–1581
10. Smith JN, Barsanti KC, Friedli HR, Ehn M, Kulmala M, Collins DR, Scheckman JH, Willians BJ, McMurry PH (2010) Proc Natl Acad Sci USA 107:6634–6639
11. Nadykto AB, Yu F, Jakovleva MV, Herb J, Xu Y (2011) Entropy 13:554–569
12. Loukonen V, Kurten T, Ortega I, Vehkamäki H, Padua A, Sellegri K, Kulmala M (2010) Atmos Chem Phys 10:4961–4974
13. Kanakidou M, Seinfeld JH, Pandis SN, Barnes I, Dentener FJ, Facchini MC, Van Dingenen R, Ervens B, Nenes A, Nielsen CJ, Swietlicki E, Putaud JP, Balkanski Y, Fuzzi S, Horth J, Moortgat GK, Winterhalter R, Myhre CEL, Tsigaridis K, Vignati E, Stephanou EG, Wilson J (2005) Atmos Chem Phys 5:1053–1123
14. Pope CA III, Ezzati M, Dockery DW (2009) N Engl J Med 360:376–386
15. Cadle SH, Mulawa PA (1980) Environ Sci Technol 14:718–723
16. Nielsen CJ, Herrmannb H, Wellerb C (2012) Chem Soc Rev 41:6684–6704
17. Fostaas B, Gangstad A, Nenseter B, Pedersen S, Sjoevoll M, Soerensen AL (2011) Energ Procedia 4:1566–1573
18. Schade GW, Crutzen PJ (1995) J Atmos Chem 22:319–346
19. Facchini MC, Decesari S, Rinaldi M, Carbone C, Finessi E, Mircea M, Fuzzi S, Moretti F, Tagliavini E, Ceburnis D, O'Dowd CD (2008) Environ Sci Technol 42:9116–9121
20. Leach J, Blanch A, Bianchi AC (1999) Atmos Environ 33:4309–4325
21. Salo K, Westerlund J, Andersson PU, Nielsen C, D'Anna B, Hallquist M (2011) J Phys Chem A 115:11671–11677
22. Frisch MJ et al. (2009) Gaussian 09 (Revision B.01). Gaussian Inc, Wallingford, CT
23. Zhao Y, Truhlar DG (2004) J Phys Chem A 108:6908–6918
24. Zhao Y, Schultz NE, Truhlar DG (2006) J Chem Theor Comput 2:364–382
25. Chandra AK (2012) J Mol Model 18:4239–4247
26. Gonzalez C, Schlegel HB (1989) J Chem Phys 90:2154–2161
27. Curtiss LA, Raghavachari K, Pople JA (1993) J Chem Phys 98:1293–1298
28. In NIST Chemistry Web Book, NIST Standard Reference Database Number 69, Release (Constants of Diatomic Molecules data compiled by K.P. Huber and G. Herzberg), website: http://www.ccbdb.nist.gov/, 2005
29. Kuchitsu K (1998) Structure of free polyatomic molecules basic data. Springer, Berlin, 1:58
30. Becke AD (1993) J Chem Phys 98:1372–1377
31. Pople JA, Head-Gordon M, Raghavachari K (1987) J Chem Phys 87:5968–5975
32. Zhurko G, Zhurko D (2011) ChemCraft 1.6
33. Hammond GS (1955) J Am Chem Soc 77:334–338
34. Shimanouchi T ((1972)) In: Tables of molecular vibrational frequencies consolidated, vol 1, National Bureau of Standards, U.S. GPO, Washington, DC
35. Galano A, Alvarez-Idaboy JR (2008) J Chem Theor Comput 4:322–327
36. Yang L, Liu JY, Wang L, He HQ, Wang Y, Li ZS (2008) J Comput Chem 29:550–561
37. Wu JY, Liu JY, Li ZS, Sun CC (2003) J Chem Phys 118:10986–10995
38. Truhlar DG, Garrett BC, Klippenstein SJ (1996) J Phys Chem 100:12771–12800
39. Wigner EP (1932) Z Phys Chem B19:203–216
40. Koch R, Kruger HU, Elend M, Palm WU, Zetzsch C (1996) Int J Chem Kinet 28:807–815